Hindawi Publishing Corporation
Journal of Applied Mathematics
Volume 2015, Article ID 238730, 9 pages
http://dx.doi.org/10.1155/2015/238730

Research Article

Magnetic and Mechanical Properties of Deformed Iron Nitride γ'-Fe_4N

Chin-Hsiang Cheng,[1] Minh-Tien Nguyen,[1] Tzong-Shyng Leu,[1] I-Ling Chang,[2] Ming-Liang Liao,[3] Sergey V. Panin,[4] and Alexey V. Panin[5]

[1]*Department of Aeronautics and Astronautics, National Cheng Kung University, Tainan 70101, Taiwan*
[2]*Department of Mechanical Engineering, National Cheng Kung University, Tainan 70101, Taiwan*
[3]*Department of Aircraft Engineering, Air Force Institute of Technology, Kaohsiung 82047, Taiwan*
[4]*Laboratory of Polymeric Composite Materials, ISPMS SB RAS, Tomsk 634021, Russia*
[5]*Laboratory of Physics of Surface Phenomena, ISPMS SB RAS, Tomsk 634021, Russia*

Correspondence should be addressed to Chin-Hsiang Cheng; chcheng@mail.ncku.edu.tw

Received 23 May 2015; Revised 19 July 2015; Accepted 26 July 2015

Academic Editor: Tao Liu

The present study is aimed at magnetic and mechanical properties of iron nitride (γ'-Fe_4N) with elastic deformation. Electronic structure and thermal properties of the iron nitride are also studied to have a comprehensive understanding of the characteristics of γ'-Fe_4N. This study is focused on the variation of the magnetic and the mechanical properties of iron nitride with a change in crystal size represented by lattice constant. As the lattice constant is altered with deformation, magnetic moment of Fe-II atoms is appreciably elevated, while that of Fe-I atoms is nearly unchanged. Dependence of the magnetic moment and the bulk modulus on the lattice constant is examined. Meanwhile, chemical bonds between Fe atoms and N atoms formed across the crystal have been visualized by delocalization of atomic charge density in electron density map, and thermodynamic properties, including entropy, enthalpy, free energy, and heat capacity, are evaluated.

1. Introduction

Iron-based nitrides received much attention from related researchers in recent years due to their interesting properties and their possible applications as high-density magnetic recording materials, as described by Shi et al. [1]. In particular, these compounds exhibited many unique characteristics in chemical, thermal, mechanical, electrical, and magnetic properties. On the other hand, in recent years highly sensitive magnetic strain gauges have been developed. In a typical magnetic sensing device, the strain gauge senses the magnetic property (such as magnetic moment and magnetic force) of the magnetic materials which responds to the physical quantity, such as strain. Through the calibration for the relationship between the magnetic property and strain, the input signal of the magnetic property can be converted to a reading of the deformation or other sensed physical quantity. Among these compounds, γ'-Fe_4N is placed on the focus of interest for applications in magnetic sensing devices. In the report of Mohn and Matar [2], its large magnetic moment, low coercive force, corrosion resistance, and chemical stability have been studied based on an ab initio calculation. However, to the best of authors' knowledge, when the material is subject to a compressive or tensile deformation, the magnetic properties of the deformed iron nitride have been not yet calculated. Therefore, it is worthwhile to perform these calculations of dependence of the magnetic moment on the deformation of iron nitride.

As a matter of fact, as mentioned by Jang et al. [3] and y Blancá et al. [4], in addition to serving as a magnetic material, iron nitride has also been considered as a ductile and damage-tolerant material because of its high bulk modulus, shear modulus, and Poisson's ratio. Recently, Takahashi et al. [5] and Yang et al. [6] presented information for mechanical

properties of the material. In parallel, investigation of thermodynamic properties such as phonon dispersion, specific heats, thermal expansion, and heat conduction is performed by Baroni et al. [7]. Unfortunately, it remains insufficient in spite of the importance of the thermodynamic properties which are the basis of solid state science and industrial applications. Thus, it is necessary to have a comprehensive understanding about these properties.

In the present study, the magnetic and the mechanical properties of iron nitride that is experiencing elastic deformation are predicted by means of the ab initio methods. Electronic structure and thermal properties of the iron nitride are also studied to have a comprehensive understanding of the characteristics of γ'-Fe_4N. This study is focused on the changes in the magnetic and the mechanical properties of iron nitride with a change in crystal size represented by lattice constant. Therefore, the opportunity of development of a nanoscale magnetic sensor for tensile or compressive strain detection based on measurement of variation in the magnetic properties of γ'-Fe_4N due to deformation may be explored. Meanwhile, electronic structure and thermal properties of the iron nitride are also studied to develop a comprehensive understanding of the characteristics of γ'-Fe_4N and also partly confirm the existing experimental results that were presented in previous reports.

Structure of iron nitride (γ'-Fe_4N) is a simple cubic crystal in the space group $Pm\bar{3}m$, as shown in Figure 1. The unit cell can be described as a variant of face center cubic structure (FCC) composed of Fe and N atoms, with one nitrogen atom at the unit center, one Fe atom (Fe-I) at corner of cubic $m\bar{3}m$ site, and 3 Fe atoms (Fe-II) at a tetragonal 4/mmm site. A more recent phase diagram of iron nitrides extended to low temperatures was proposed by Du Marchie van Voorthuysen et al. [8]. Depending on the nitrogen content, different iron nitride phases with different structures and properties can be observed. All iron nitrides are metallic conductors which are metastable with respect to decomposition into Fe and N_2. According to the phase diagram provided by authors, γ'-Fe_4N phase is located in a narrow composition range at around 20% atomic percent nitrogen. The phase of γ'-Fe_4N features remarkable magnetic properties, which make it attractive as used in a multilayer structure designed for magnetic and electronic devices.

2. Computational Methods

In condensed matter physics, the material property is predicted based on the information of interacting electrons and atomic nuclei. They could be found by using suitable computational tools in quantum mechanics. The idea of the electron density methods was firstly presented by Hohenberg and Kohn [9]. According to their study, the ground state properties of the molecular system can be yielded without calculating the complicated wave function. This method was then called density functional theory (DFT) that results in a major scientific breakthrough by solving the complexity of material problems. The calculation of the properties is based on the ab initio electronic structure method derived from spin-polarized density functional theory and plane

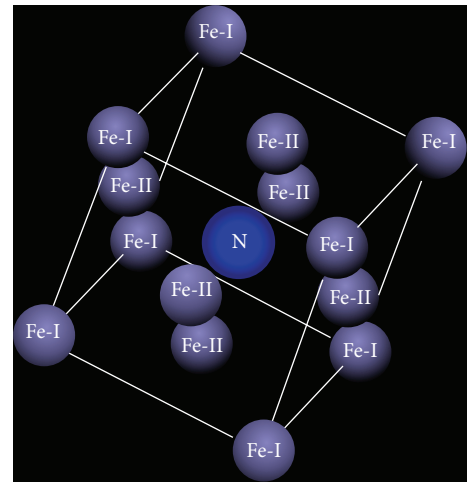

Figure 1: Unit cell structure of γ'-Fe_4N.

wave pseudopotential method used by Baroni et al. [7]. Ultrasoft pseudopotentials are used to describe the interactions between electrons and core ions, as suggested by Li et al. [10] and Soni et al. [11]. Pseudo atomic calculation is performed for N-$2s^2 2p^3$ and Fe-$3d^6 4s^2$ electronic configurations. The exchange-correlation potential is applied with the generalized gradient approximation (GGA) based on the Perdew-Burke-Ernzerhof (PBE) expression. The geometry optimizations and property calculations are performed by Broyden-Fletcher-Goldfarb-Shanno (BFGS) method.

The computation is performed on the framework of a commercial code, CASTEP [12]. The calculations are iterated toward self-consistency with the atom convergence total energy criterion of 0.5×10^{-6} eV/atom. The final set of the cutoff energy is 330 eV with $8 \times 8 \times 8$ k-points in Monkhorst-Pack grid [11]. Atomic relaxations continue until the maximum stress and the force are less than 0.02 GPa and 0.01 eV/Å, respectively.

Magnetism in the solid state involves a large variety of phenomena that can be characterized by the magnetic moment, which is the quantity of major concern here. For a magnetic system, the magnetization density $\mathbf{m}(\mathbf{r})$ is a property that can be obtained directly from spin-polarized DFT as follows:

$$\mathbf{m}(\mathbf{r}) = -\mu_B \sum_{\alpha,\beta} \Psi_\alpha^* (\mathbf{r})\, \sigma_{\alpha,\beta} \Psi_\beta (\mathbf{r}), \tag{1}$$

where Bohr magnetron μ_B is defined as

$$\mu_B = \frac{e\hbar}{2m_e c} \tag{2}$$

and e is the elementary charge (1.602×10^{-19} C); $\hbar$ is the reduced Planck constant (1.055×10^{-34} J·s); m_e is the electron rest mass (9.1×10^{-31} kg); c is the speed of light; and Pauli matrices are denoted by

$$\sigma_x = \begin{pmatrix} 0 & 1 \\ 1 & 0 \end{pmatrix};$$

$$\sigma_y = \begin{pmatrix} 0 & -1 \\ 1 & 0 \end{pmatrix};$$

$$\sigma_z = \begin{pmatrix} 1 & 0 \\ 0 & -1 \end{pmatrix}. \tag{3}$$

The Kohn-Sham orbitals $\psi_i(r)$ are related to the electron density of N electrons by

$$\rho(r) = \sum_{i}^{N} \sum_{S} \left|\psi_i(r)\right|^2, \quad i = 1 \text{ to } N. \tag{4}$$

The N orbitals $\psi_i(r)$ are obtained by solving the Kohn-Sham orbital equations in canonical form, as described by Kronmüller and Parkin [13]. The spin magnetic moment is the magnetic moment induced by the spin of elementary particles, which is calculated by

$$m_{\text{spin}} = \left|\int \mathbf{m}(\mathbf{r})\, d\mathbf{r}\right| = \left|\int \left[\rho_{\uparrow}(\mathbf{r}) - \rho_{\downarrow}(\mathbf{r})\right] d\mathbf{r}\right|, \tag{5}$$

where $\rho_{\uparrow}(\mathbf{r})$ and $\rho_{\downarrow}(\mathbf{r})$ represent the spin-up and spin-down electron density functions, respectively.

The magnetization density defined by (1) is a consequence of the imbalance of electrons spin-up or spin-down; therefore, the quantity defined in (5) is called spin magnetic moment. According to electronic population analysis by Mulliken [14], the spin magnetic moment should be introduced to each atom in the unit cell.

The energy changes due to deformation of the lattice vectors have been studied when the elastic properties of the crystal are analyzed. The deformation can occur under influence of stresses exerted on the crystal. As discussed by Gressmann et al. [15], by using Voigtian matrix formulation of Hooke's law, the strain tensors are characterized by matrix of six components ε_i as

$$\boldsymbol{\varepsilon} = \begin{pmatrix} \varepsilon_1 & \frac{\varepsilon_6}{2} & \frac{\varepsilon_5}{2} \\ \frac{\varepsilon_6}{2} & \varepsilon_2 & \frac{\varepsilon_4}{2} \\ \frac{\varepsilon_5}{2} & \frac{\varepsilon_4}{2} & \varepsilon_3 \end{pmatrix}. \tag{6}$$

Lattice vectors **a**, **b,** and **c** at the equilibrium state will be changed to $\mathbf{a}'$, $\mathbf{b}'$, and $\mathbf{c}'$, respectively, after deformation. For cubic lattice,

$$\mathbf{R} = \begin{pmatrix} \mathbf{a} & 0 & 0 \\ 0 & \mathbf{b} & 0 \\ 0 & 0 & \mathbf{c} \end{pmatrix},$$

$$\mathbf{R}' = \begin{pmatrix} \mathbf{a}' & 0 & 0 \\ 0 & \mathbf{b}' & 0 \\ 0 & 0 & \mathbf{c}' \end{pmatrix}, \tag{7}$$

where matrix $\mathbf{R}'$ is expressed in terms of the deformed lattice vectors $\mathbf{a}'$, $\mathbf{b}'$, and $\mathbf{c}'$. One then has

$$\mathbf{R}' = \mathbf{R}(\mathbf{1} + \boldsymbol{\varepsilon}), \tag{8}$$

where **1** is a unit matrix.

For the cubic crystal, the elastic constants matrix can be written as

$$\begin{pmatrix} C_{11} & C_{12} & C_{12} & 0 & 0 & 0 \\ C_{12} & C_{11} & C_{12} & 0 & 0 & 0 \\ C_{12} & C_{12} & C_{11} & 0 & 0 & 0 \\ 0 & 0 & 0 & C_{44} & 0 & 0 \\ 0 & 0 & 0 & 0 & C_{44} & 0 \\ 0 & 0 & 0 & 0 & 0 & C_{44} \end{pmatrix}. \tag{9}$$

In theory, the change in the elastic energy per unit cell $(E - E_0)$ is related to the components of the strain tensor and the elastic stiffness tensor by

$$E - E_0 = \frac{1}{2} V_0 \sum_{1}^{6} C_{ij} \varepsilon_i \varepsilon_j. \tag{10}$$

Because of symmetry of the cubic crystal γ'-Fe_4N, only the three independent elastic constants, C_{11}, C_{12}, and C_{44}, exist. The elastic constants can be calculated in terms of various strain-energy states on the crystal:

(1) Imposing an isotropic state of strain with $\varepsilon_1 = \varepsilon_2 = \varepsilon_3 = \varepsilon$ and all other strains $\varepsilon_i = 0$, the relationship between V_0 and strain ε is described by

$$\varepsilon = \frac{(1/3)(V - V_0)}{V_0}. \tag{11}$$

Equation (10) becomes

$$E - E_0 = \frac{3}{2} V_0 (C_{11} + 2C_{12}) \varepsilon^2 = \frac{9}{2} V_0 B \varepsilon^2 = \frac{(1/2) B (V - V_0)}{V_0} \tag{12}$$

which allows us to determine the sum of the elastic constants $(C_{11} + 2C_{12})$ based on the values of V_0, E_0, and total energy data calculated for different V (or ε). Then, the bulk modulus B can be determined by

$$B = \frac{1}{3}(C_{11} + 2C_{12}). \tag{13}$$

(2) Imposing a uniaxial state of strain $\varepsilon_1 = \varepsilon$ and all other strains $\varepsilon_i = 0$, (10) then becomes

$$E - E_0 = \frac{1}{2} V_0 C_{11} \varepsilon^2 \tag{14}$$

which leads to determination of the elastic constant C_{11}.

(3) Imposing a shear strain $\varepsilon_4 = \varepsilon$ and all other strains $\varepsilon_i = 0$, (10) then becomes

$$E - E_0 = \frac{1}{2} V_0 C_{44} \varepsilon^2 \tag{15}$$

which leads to determination of the elastic constant C_{44}.

Based on the obtained elastic constants, C_{11}, C_{12}, and C_{44}, the following mechanical properties can be further determined as follows:

(1) Elastic compliances:

$$S_{11} = \frac{C_{11} + C_{12}}{C_{11}^2 + C_{11}C_{12} - C_{12}^2}, \tag{16a}$$

$$S_{12} = \frac{-C_{12}}{C_{11}^2 + C_{11}C_{12} - C_{12}^2}, \tag{16b}$$

$$S_{44} = \frac{1}{C_{44}}. \tag{16c}$$

(2) Elastic anisotropy:

$$A = \frac{2C_{44}}{C_{11} - C_{12}}. \tag{17}$$

(3) Young's modulus:

$$E = \frac{9BG}{(G + 3B)}. \tag{18}$$

(4) Shear modulus:

$$G = \frac{C_{11} - C_{12} + 3C_{44}}{5}. \tag{19}$$

(5) Poisson's ratio:

$$\nu = \frac{3B - 2G}{2(3B + G)}. \tag{20}$$

The phonon-related thermodynamic properties such as enthalpy (H), entropy (S), free energy (F), and lattice heat capacity (C_v) are computed in a quasiharmonic approximation:

(1) Enthalpy:

$$H(T) = E_{\text{tot}} + E_{\text{zp}} + \int \frac{\hbar\omega}{e^{\hbar\omega/kT} - 1} F(\omega)\, d\omega, \tag{21}$$

where E_{zp} is the zero-point vibrational energy, k is Boltzmann's constant, $\hbar$ is reduced Planck's constant, and $F(\omega)$ is the phonon density of states. E_{zp} can be evaluated as

$$E_{\text{zp}} = \frac{1}{2} \int F(\omega)\, \hbar\omega\, d\omega. \tag{22}$$

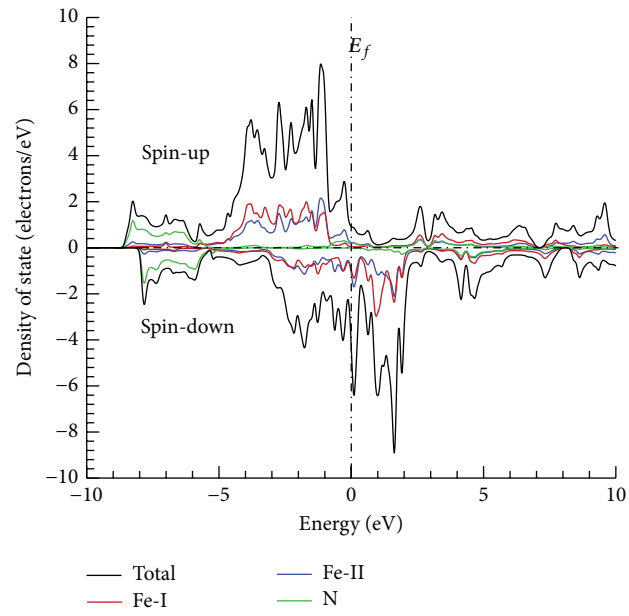

FIGURE 2: Total and partial density of state at $a = 3.772$ Å.

(2) Free energy:

$$F(T) = E_{\text{tot}} + E_{\text{zp}} + kT \int F(\omega) \ln\left(1 - e^{-\hbar\omega/kT}\right) d\omega. \tag{23}$$

(3) Entropy:

$$S(T) = k \left[\int \frac{\hbar\omega/kT}{e^{\hbar\omega/kT} - 1} F(\omega)\, d\omega - \int F(\omega) \ln\left(1 - e^{-\hbar\omega/kT}\right) d\omega \right]. \tag{24}$$

(4) Lattice heat capacity:

$$C_V(T) = k \int \frac{(\hbar\omega/kT)^2\, e^{\hbar\omega/kT}}{e^{\hbar\omega/kT} - 1} F(\omega)\, d\omega. \tag{25}$$

3. Results and Discussion

3.1. Magnetic Properties and Electronic Structure. Previous experimental information for lattice constant presented by Li et al. [10] is used in the geometry optimization process to get the relaxed structures. Numerical prediction of the lattice constant of the iron nitride after optimization is found to be 3.772 Å, which is only slightly lower than the experimental value 3.79 Å [10] by 0.5%.

Total density and partial density of state of iron nitride are displayed in Figure 2. The number of spin-up (↑) electrons exceeds that of spin-down (↓) electrons so that the distribution of DOS is asymmetric and ferromagnetism of the material is hence induced. The total DOS lies between −9 eV and the Fermi level (E_f). For the nitrogen atom, it is between −9 and −5.2 eV and for Fe-I atom it is between −5 eV and E_f. These results indicate a strong superposition

Table 1: Partial density of state of γ'-Fe_4N at $a = 3.772$ Å.

Atom	Present study	Rebaza et al. [16]
Fe-I	−5 eV to E_f	−5 eV to E_f
Fe-II	−9 eV to E_f	−8.5 eV to E_f
N	−9 eV to −5.5 eV	−8.5 eV to −5.3 eV

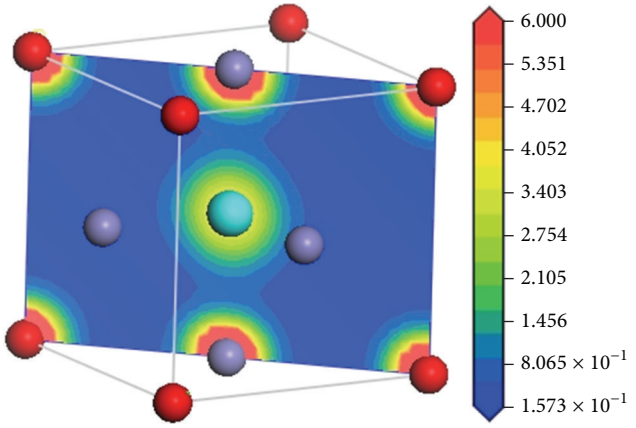

Figure 3: Total electron density map on the tridiagonal plane with Fe-I and N atoms at $a = 3.772$ Å.

of electronic state of the nitrogen atom and Fe-II atom in the range between −9 and −5.2 eV and explain the reason for the difference between Fe-I and Fe-II magnetic moments in terms of the Fe-N 3d-sp hybridization mentioned by Rebaza et al. [16]. As shown in Table 1, the obtained results closely agree with the theoretical data presented by Rebaza et al. [16].

Distribution of the total electron density on the tridiagonal plane in the unit cell is plotted in Figure 3. It is found that the interaction between atoms N and Fe-I is very weak. Meanwhile, both Fe-I atoms and Fe-II atoms contribute electrons to the total electron density of crystal but major contribution is from the Fe-I atoms. Similarly, Figure 4 conveys the difference of electron density from each atom. As expected, nitrogen attracts electrons from neighboring Fe atoms, and these electrons are incompletely screened and affect the magnetic moment. The increment of electrons is concentrated on the N atom.

Effective ionic valences listed in Table 2 are defined to be the difference between the formal ionic charge and the Mulliken charge. It is also used as a measure of ionic bond. A positive value indicates an ideal ionic bond with increasing levels of covalence on the anion species in the crystal. Table 2 shows the overlap populations for nearest neighbors in the crystal. The positive and negative values indicate bonding and antibonding states, respectively, and a value close to zero indicates insignificant interaction between the electronic populations of the two atoms. Furthermore, a high overlap population indicates a high degree of covalence in the bond. In fact, the bonding types include covalent, ionic, and metallic characters. It is found that the atoms at the cubic corners, Fe-I, have a low net charge (−0.06 eV), whereas the Fe-I–Fe-II bond has high overlap populations. This implies that

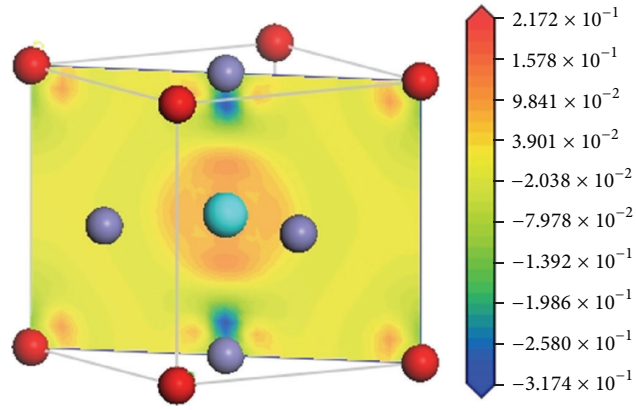

Figure 4: Electron density difference map of the tridiagonal plane with Fe-I and N bonds at $a = 3.772$ Å.

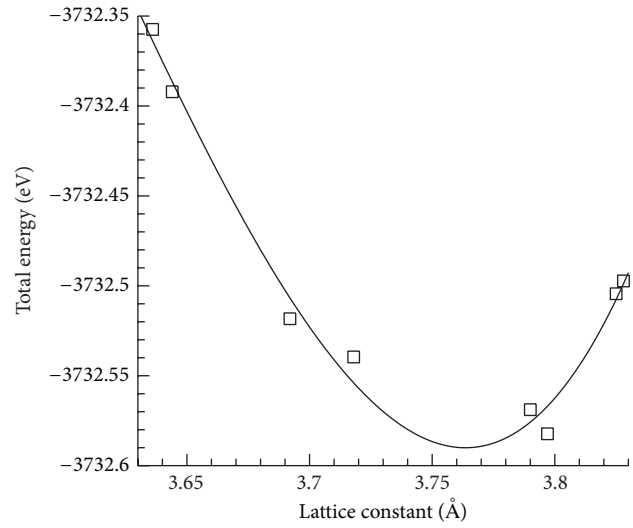

Figure 5: Dependence of total energy on lattice constant.

the bonds apparently have metallic character. The numbers of valence electrons of Fe are not integer, which means that the cohesive bond is no longer purely metallic. A nonmetallic component, ionic or covalent, has been added to it.

Dependence of the total energy on the lattice constant is displayed in Figure 5. To investigate the sensitivity of the total energy and the magnetic moment to lattice constant with deformation, the quantities are calculated at different lattice constants a varied from 3.636 to 3.828 Å. As a result, the total energy can be correlated to the lattice constant with a quadratic-form relation (see Figure 5). In Figure 5, it is seen that the total energy reaches its minimum at $a = 3.765$ Å. The quadratic-form relation reflects the total energy change in response to a deformation of the material.

Figure 6 shows the dependence of the magnetic moment of Fe-I and Fe-II atoms on lattice constant. It is noticed that the effects of the lattice constant are remarkable on the magnetic moment of Fe-II atoms. The magnetic moment of Fe-II increases greatly with the lattice constant. In other words, by measuring the variation in magnetic properties

Table 2: Atomic Mulliken charges and overlap population of bonds in γ'-Fe_4N at $a = 3.772$ Å.

Atom	Mulliken charge ($\|e\|$)	Effective valence ($\|e\|$)	Bond	Overlap populations ($\|e\|$)	Bond length (Å)
N	5.75	−0.75	(N)–(Fe-II)	0.62	1.895
Fe-II	7.73	0.27	(Fe-II)–(Fe-II)	−0.54	2.67993
Fe-I	8.06	−0.06	(Fe-I)–(Fe-II)	0.53	2.67993

Table 3: A comparison in magnetic moments of γ'-Fe_4N between present numerical and previous experimental or theoretical data [16–19], at $a = 3.772$ Å.

	Present study	Previous experimental results [17]	Previous theoretical results [16, 18, 19]
$m_{\text{Fe-I}}$ (μ_B)	2.98	3.0 [17]	2.84 [16], 3.09 [18], and 2.98 [19]
$m_{\text{Fe-II}}$ (μ_B)	2.3	2.0 [17]	2.27 [16], 2.11 [18], and 2.23 [19]

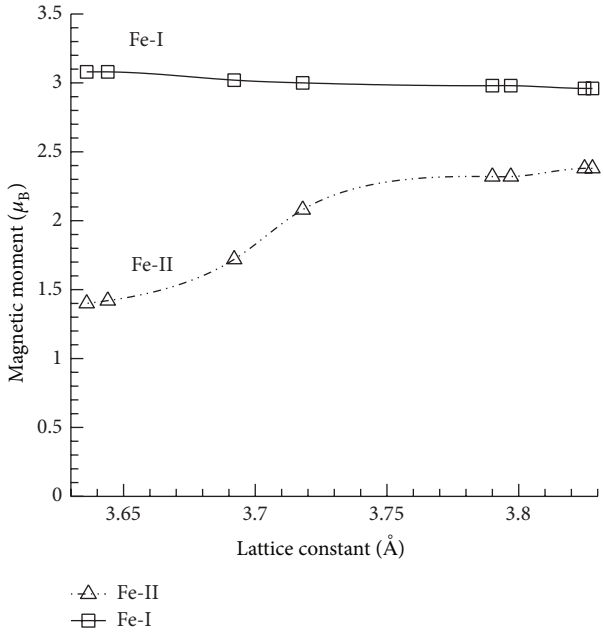

Figure 6: Dependence of magnetic moment of Fe-I and Fe-II atoms on lattice constant.

of the Fe-II atoms with the lattice constants, it is possible to develop a nanoscale magnetic sensor for tensile or compressive strain detection. However, the effects of the lattice constant are relatively inappreciable on the magnetic moment of Fe-I atoms. It is seen that the magnetic moment of Fe-I atom is only slightly decreased as a is increased from 3.636 to 3.828 Å. The increased distance between the magnetic atoms due to deformation leads to electrons transferring from the 3d spin-down (↓) band to the 3d spin-up (↑) band. Note that the variation of the magnetic moment may be attributed to the effect of the hybridization of the interstitial N atoms with the neighboring Fe atoms, which is a straightforward consequence of the deformation.

A comparison in the magnetic moments of γ'-Fe_4N between the present predictions and some existing information [16–19] is made to ensure accuracy of the numerical simulation. The results are provided in Table 3. For the case at $a = 3.772$ Å shown in this table, the present numerical predictions of the magnetic moments are 2.98 μ_B and 2.3 μ_B for the Fe-I and Fe-II atoms, respectively. These values closely agree with the existing information.

3.2. Mechanical Properties. The elastic properties of γ'-Fe_4N are evaluated at various strain magnitudes to ensure that the computation results are independent of the magnitude of strain to a certain extent. The obtained elastic constants C_{11}, C_{12}, and C_{44} and the results of elastic properties are given in Table 4. It is found that, at $a = 3.772$ Å, Young's modulus (E) of γ'-Fe_4N is 176.5 GPa, which is roughly 12–17% lower than those of α-Fe (211 GPa) reported in [20] and of γ-Fe austenitic stainless steels (200 GPa) reported in [21]. It is interesting to note that γ'-Fe_4N is more elastically compliant than γ-Fe austenitic stainless steels in spite of their structural similarity. Since γ'-Fe_4N is ferromagnetic while γ-Fe austenitic stainless steels are paramagnetic at room temperature, the difference in magnetic configuration between γ'-Fe_4N and γ-Fe austenitic stainless steels may be responsible for the decrease in stiffness associated with addition of N atom to FCC γ-Fe. The dependence of the lattice volume on the magnetization is known as the magneto-volume effect. The volume expansion of γ'-Fe_4N due to its ferromagnetism may cause the reduction in elastic modulus, compared to paramagnetic γ-Fe austenitic stainless steels.

The shear modulus of γ'-Fe_4N (G) is also evaluated in the present study. The shear modulus is of significance in plastic deformation of materials since it is linked to the strength and hardness of materials. For instance, the ideal shear strength of material is assumed to be proportional to its shear modulus. In accordance with the numerical simulation, the shear modulus of γ'-Fe_4N is predicted to be 65.8 GPa. On the other hand, the shear modulus of γ-Fe is 49 GPa. This implies that γ'-Fe_4N is intrinsically at least 1.3 times stronger than γ-Fe regarding plastic deformation.

Figure 7 shows the dependence of the bulk modulus on the lattice constant. It is seen that the bulk modulus of the unit cell structure of γ'-Fe_4N is rather sensitive to the lattice constant. As the lattice constant is varied from 3.7 to 3.797 Å, the bulk modulus is decreased from 320 to 164 GPa. It means that the mechanical properties of γ'-Fe_4N could be greatly altered while the bulk material suffers from a deformation.

Table 4: Mechanical properties of γ'-Fe_4N, at $a = 3.772$ Å.

C_{11} (GPa)	C_{12} (GPa)	C_{44} (GPa)	S_{11} (10^{-3} GPa^{-1})	S_{12} (10^{-3} GPa^{-1})	S_{44} (10^{-3} GPa^{-1})	A	B (GPa)	E (GPa)	G (GPa)	ν
303	126	50.7	3.76	−1.1	1.97	0.57	185	176.5	65.8	0.36

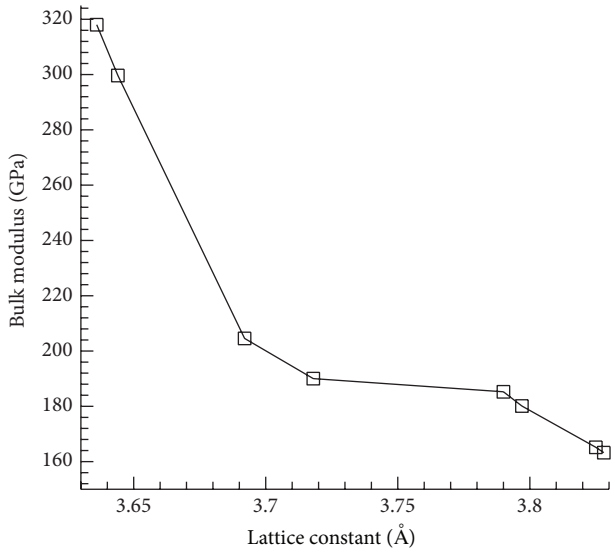

Figure 7: Dependence of bulk modulus on lattice constant.

3.3. Thermodynamic Properties. The temperature-dependent thermodynamic properties, enthalpy $H(T)$, entropy $S(T)$, free energy $F(T)$, and heat capacity $C_v(T)$, are plotted in Figure 8. Since the Helmholtz free energy is defined by $F = H - TS$, the property entropy is presented in the form of $T \times S$ product to allow comparison among the quantities F, H, and TS in the same dimension eV. It is observed in Figure 8(a) that, at a temperature lower than 100 K, magnitudes of enthalpy, entropy, and free energy are all nearly zero. However, as the temperature is above 100 K, a further increased temperature leads to a significant increase in both H and TS but a decrease in free energy F.

Variation of the heat capacity C_v with temperature is illustrated in Figure 8(b). It is found that the heat capacity increases dramatically with temperature. Below a critical temperature of around 700 K, C_v increases very rapidly with temperature. As the temperature is higher than the critical temperature, C_v increases gradually and approaches the Dulong and Petit limit yielded by harmonic approximation of the Debye model.

4. Concluding Remarks

The present study is concerned with magnetic and mechanical properties of iron nitride (γ'-Fe_4N) with elastic deformation. The investigation is focused on the variation of the magnetic and the mechanical properties of iron nitride with a change in crystal size represented by lattice constant. The computation is based on ab initio electronic structure analysis and derived by spin-polarized density functional theory (DFT).

According to the numerical predictions, the following conclusions can be made:

(1) The present numerical results have been compared with the existing information extensively. For example, the obtained results agree closely with the existing data for the lattice constant presented by Li et al. [10], for the partial density data presented by Rebaza et al. [16] and for the magnetic moments data presented in [16–19]. The accuracy of the present predictions can be ensured.

(2) At $a = 3.772$ Å, the magnetic moment is found to be $2.98\,\mu_B$ and $2.3\,\mu_B$ for Fe-I and Fe-II atoms, respectively. When the lattice constant is increased with deformation, magnetic moment of Fe-II atoms is appreciably elevated, while that of Fe-I atoms is only slightly decreased as a is varied between 3.636 and 3.828 Å. In other words, by measuring the variation in magnetic properties of the Fe-II atoms with the lattice constants, it is possible to develop a nanoscale magnetic sensor for tensile or compressive strain deformation.

(3) It is noticed that the bulk modulus of the unit cell structure of γ'-Fe_4N is rather sensitive to the lattice constant. As the lattice constant is varied from 3.7 to 3.797 Å, the bulk modulus is decreased from 320 to 164 GPa. It means that the mechanical properties of γ'-Fe_4N could be greatly altered while the bulk material suffers from a deformation.

(4) In addition, the thermodynamic properties of γ'-Fe_4N, including entropy, enthalpy, free energy, and heat capacity, are calculated. For entropy, enthalpy, and free energy, temperature of 100 K appears to be a critical temperature. At a temperature lower than 100 K, magnitudes of enthalpy, entropy, and free energy are all nearly fixed at zero. However, as the temperature is above 100 K, a further increased temperature leads to a significant increase in both H and S but a decrease in free energy. On the other hand, a monotonic increase in heat capacity C_v with temperature is observed. It is found that as the temperature is over 700 K, the value of heat capacity gradually approaches the Dulong and Petit limit.

Nomenclature

a:	Lattice constant, Å
a, **b**, and **c**:	Lattice vectors before deformation
a′, **b′**, and **c′**:	Lattice vectors after deformation
A:	Elastic anisotropy
B:	Bulk modulus, GPa
c:	Speed of light, m/s

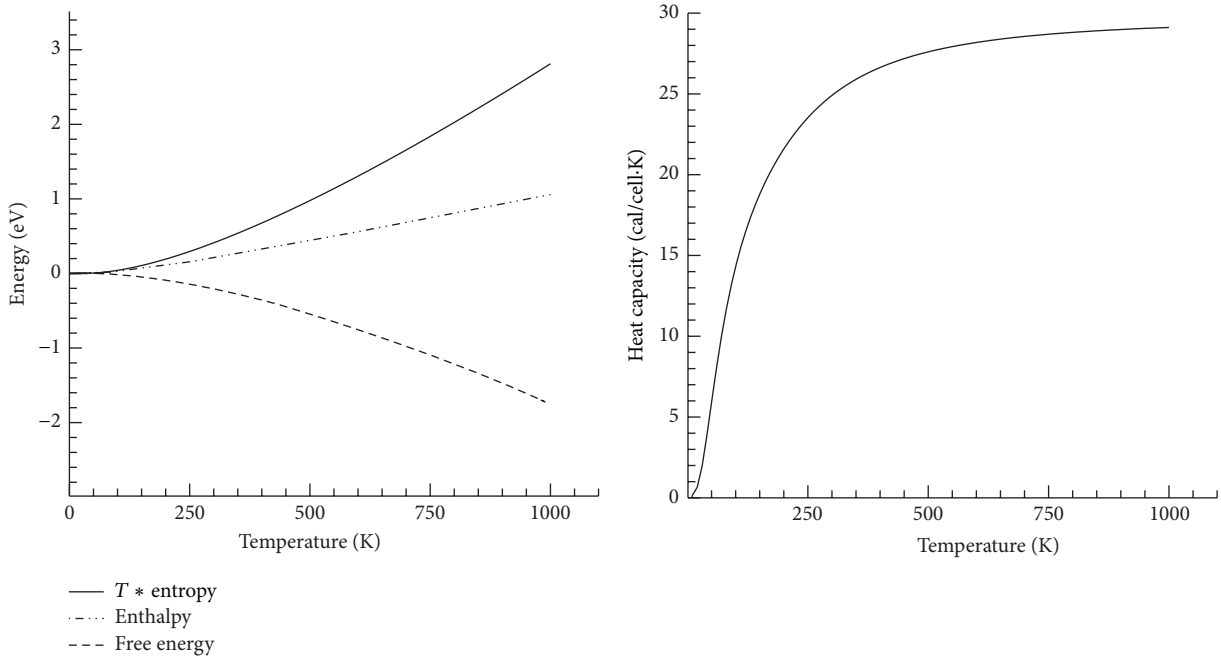

(a) TS, H, and F (b) C_v

Figure 8: Temperature dependence of thermodynamic properties at $a = 3.772$ Å.

C: Elastic constant, GPa
$C_v(T)$: Heat capacity, cal/(cell·K)
e: Elementary charge, 1.602×10^{-19} C
E: Young's modulus, GPa
E_f: Fermi level energy, eV
$F(T)$: Free energy, eV
G: Shear modulus, GPa
$\hbar$: Reduced Planck constant, 1.055×10^{-34} J·s
H: Enthalpy, kJ/kg
m: Magnetic moment, μ_B
m_e: Electron rest mass, 9.1×10^{-31} kg
m_{spin}: Spin magnetic moment, μ_B
$\mathbf{m}(\mathbf{r})$: Magnetization density
N: Number of electrons
$\mathbf{r}$: Electron position vector, Å
$\mathbf{R}$: Lattice vector matrix before deformation
$\mathbf{R}'$: Lattice vector matrix after deformation
S: Elastic compliance, 10^{-3} GPa^{-1}
$S(T)$: Entropy, kJ/(kg·K)
T: Temperature, K
ν: Poisson's ratio.

Greek Symbols

ε: Strain component
$\boldsymbol{\varepsilon}$: Strain vector
μ_B: Bohr magnetron
ρ: Electron density
σ: Pauli matrix
ν: Poison's ratio
ψ: Kohn-Sham orbital function.

Conflict of Interests

The authors declare that there is no conflict of interests regarding the publication of this paper.

Acknowledgments

This research received funding, in part, from the Headquarters of University Advancement at National Cheng Kung University, which is sponsored by the Ministry of Education, Taiwan. The authors also appreciate the financial support from Ministry of Science and Technology, Taiwan, under Grant 103-2923-E-006-004-MY3.

References

[1] Y. J. Shi, Y. L. Du, and G. Chen, "Ab initio study of structural and magnetic properties of cubic $Fe_4N(0\ 0\ 1)$ surface," *Solid State Communications*, vol. 152, no. 16, pp. 1581–1584, 2012.

[2] P. Mohn and S. F. Matar, "The γ-Fe_4N system revisited: an ab initio calculation study of the magnetic interactions," *Journal of Magnetism and Magnetic Materials*, vol. 191, no. 1-2, pp. 234–240, 1998.

[3] Y.-R. Jang, I. G. Kim, and J. I. Lee, "Electronic structure and magnetic properties of $Fe_4N(0\ 0\ 1)$," *Journal of Magnetism and Magnetic Materials*, vol. 263, no. 3, pp. 366–372, 2003.

[4] E. L. P. y Blancá, J. Desimoni, N. E. Christensen, H. Emmerich, and S. Cottenier, "The magnetization of γ'-Fe_4N: theory vs. experiment," *Physica Status Solidi (B)*, vol. 246, no. 5, pp. 909–928, 2009.

[5] T. Takahashi, J. Burghaus, D. Music, R. Dronskowski, and J. M. Schneider, "Elastic properties of gamma-Fe_4N probed by

nanoindentation and ab initio calculation," *Acta Materialia*, vol. 60, pp. 2054–2060, 2012.

[6] J. Yang, H. Sun, and C. Cheng, "Anomalous strength anisotropy of γ'-Fe_4N identified by first-principles calculations," *Applied Physics Letters*, vol. 94, Article ID 151914, pp. 151914–151917, 2009.

[7] S. Baroni, S. De Gironcoli, A. Dal Corso, and P. Giannozzi, "Phonons and related crystal properties from density-functional perturbation theory," *Reviews of Modern Physics*, vol. 73, no. 2, pp. 515–562, 2001.

[8] E. H. Du Marchie van Voorthuysen, N. C. Chechenin, and D. O. Boerma, "Low-temperature extension of the Lehrer diagram and the iron-nitrogen phase diagram," *Metallurgical and Materials Transactions A*, vol. 33, no. 8, pp. 2593–2598, 2002.

[9] P. Hohenberg and W. Kohn, "Inhomogeneous electron gas," *Physical Review*, vol. 136, pp. B864–B871, 1964.

[10] H. Li, L. Zhang, Q. Zeng et al., "First-principles study of the structural, vibrational, phonon and thermodynamic properties of transition metal carbides TMC (TM = Ti, Zr and Hf)," *Solid State Communications*, vol. 151, no. 1, pp. 61–66, 2011.

[11] H. R. Soni, V. Mankad, S. K. Gupta, and P. K. Jha, "A first principles calculations of structural, electronic, magnetic and dynamical properties of mononitrides FeN and CoN," *Journal of Alloys and Compounds*, vol. 522, pp. 106–113, 2012.

[12] S. J. Clark, M. D. Segall, C. J. Pickard et al., "First principles methods using CASTEP," *Zeitschrift fur Kristallographie*, vol. 220, no. 5-6, pp. 567–570, 2005.

[13] H. Kronmüller and S. Parkin, *Handbook of Magnetism and Advanced Magnetic Materials*, vol. 1, Wiley-Interscience, 2007.

[14] R. S. Mulliken, "Electronic population analysis on LCAO–MO molecular wave functions. I," *The Journal of Chemical Physics*, vol. 23, no. 10, pp. 1833–1840, 1955.

[15] T. Gressmann, M. Wohlschlögel, S. Shang et al., "Elastic anisotropy of γ'-Fe_4N and elastic grain interaction in γ'-Fe_4N_{1-y} layers on α-Fe: first-principles calculations and diffraction stress measurements," *Acta Materialia*, vol. 55, no. 17, pp. 5833–5843, 2007.

[16] A. V. G. Rebaza, J. Desimoni, and E. L. P. y Blancá, "Study of the magnetic and electronic properties of the Fe_4N with pressure," *Physica B: Condensed Matter*, vol. 404, no. 18, pp. 2872–2875, 2009.

[17] B. C. Frazer, "Magnetic structure of Fe_4N," *Physical Review*, vol. 112, no. 3, pp. 751–754, 1958.

[18] C. A. Kuhnen, R. S. de Figueiredo, V. Drago, and E. Z. de Silva, "Mössbauer studies and electronic structure of γ'-Fe_4N," *Journal of Magnetism and Magnetic Materials*, vol. 111, no. 1-2, pp. 95–104, 1992.

[19] R. Coehoorn, G. H. O. Daalderop, and H. J. F. Jansen, "Full-potential calculations of the magnetization of $Fe_{16}N_2$ and Fe_4N," *The Physical Review B*, vol. 48, no. 6, pp. 3830–3834, 1993.

[20] W. F. Gale and T. C. Totemeier, *Smithells Metals Reference Book*, Elsevier, Oxford, UK, 2004.

[21] A. Teklu, H. Ledbetter, S. Kim, L. A. Boatner, M. McGuire, and V. Keppens, "Single-crystal elastic constants of Fe-15Ni-15Cr alloy," *Metallurgical and Materials Transactions A*, vol. 35, no. 10, pp. 3149–3154, 2004.